Revisiting Over-smoothing and Over-squashing Using Ollivier-Ricci Curvature

Anonymous Authors[1]

Abstract

Graph Neural Networks (GNNs) had been demonstrated to be inherently susceptible to the problems of over-smoothing and over-squashing. These issues prohibit the ability of GNNs to model complex graph interactions by limiting their effectiveness in taking into account distant information. Our study reveals the key connection between the local graph geometry and the occurrence of both of these issues, thereby providing a unified framework for studying them at a local scale using the Ollivier-Ricci curvature. Specifically, we demonstrate that over-smoothing is linked to positive graph curvature, while over-squashing is linked to negative graph curvature. Based on our theory, we propose the Batch Ollivier-Ricci Flow, a novel rewiring algorithm capable of simultaneously addressing both over-smoothing and over-squashing.

1. Introduction

A collection of entities with a set of relations between them is among the simplest, and yet most general, types of structure. It came as no surprise that numerous real world data are naturally represented by graphs (Harary, 1967; Hsu & Lin, 2008; Estrada & Bonchev, 2013), motivating many recent advancements in the study of Graph Neural Networks (GNNs). This has lead to a wide range of successful applications, including physical modeling (Battaglia et al., 2016; Kipf et al., 2018; Sanchez-Gonzalez et al., 2018), chemical and biological inference (Duvenaud et al., 2015; Gilmer et al., 2017), recommender systems (Berg et al., 2017; Ying et al., 2018; Fan et al., 2019; Wu et al., 2019), generative models (Li et al., 2018b; Bojchevski et al., 2018; Shi et al., 2020), financial prediction (Chen et al., 2018b; Matsunaga et al., 2019; Yang et al., 2019), and knowledge graph (Shang et al., 2019; Zhang et al., 2019).

[1]Anonymous Institution, Anonymous City, Anonymous Region, Anonymous Country. Correspondence to: Anonymous Author <anon.email@domain.com>.

Preliminary work. Under review by the International Conference on Machine Learning (ICML). Do not distribute.

Despite their success, current GNN designs suffer from two critical setbacks that prevent the widespread adoption of GNNs in practical applications. The first common problem encountered by GNNs is known as over-smoothing (Li et al., 2018a). Over-smoothing occurs when node features quickly converge to each other and become indistinguishable as the number of layers increases. This issue puts a limit on the depth of a GNN, prohibiting the model's capability of capturing complex relationships in the data. Another plight plaguing GNNs is known as over-squashing (Alon & Yahav, 2021). This phenomenon happens when the number of nodes within the receptive field of a particular node grows exponentially with the number of layers, leading to the squashing of exponentially-growing amount of information into fixed-size node features. Such over-squashing hinders the ability of GNNs to effectively process distant information and capture long-range dependencies between nodes in the graph, especially in the case of deep GNNs that require many layers.

Together, over-smoothing and over-squashing impair the performance of modern GNNs, impeding their application to many important settings that involve very large graph. (Cai & Wang, 2020; Alon & Yahav, 2021). Alleviating either of these problems has been the main focus in many recent studies of GNNs (Luan et al., 2019; Zhao & Akoglu, 2020; Topping et al., 2022). It has been noted that over-smoothing and over-squashing are somewhat related problems (Karhadkar et al., 2023). Nevertheless, to the best of our knowledge, there has been no work in the literature that offers a common framework to understand these issues, nor to rigorously study them at the local level. Such unified approach presents a potentially crucial theoretical contribution to our understanding of the over-smoothing and over-squashing issues. It enables the development of novel architectures and methods that can effectively learn complex and long-range graph interactions, thereby broadening the applications of GNNs on practical tasks.

Contribution. We present a unified theoretical framework to study both the over-smoothing and over-squashing phenomena in GNNs at the local level using the Ollivier-Ricci curvature, an inherent local geometric property of graphs. Our key contributions are three-fold:

1. We prove that very positively curved edges cause node

representations to become similar, thereby establishing a link between the over-smoothing issue and high edge curvature.

2. We prove that low curvature value characterizes graph bottlenecks and demonstrate a connection between the over-squashing issue and negative edge curvature.

3. Based on our theoretical results, we propose the Batch Ollivier-Ricci Flow (BORF), a novel curvature-based rewiring method designed to mitigate the over-smoothing and over-squashing issues simultaneously.

Organization. We structure this paper as follows: In Section 2, we give a brief summary of the relevant backgrounds in the study of GNNs and provide a concise formulation for the Ollivier-Ricci curvature on graphs. In Section 3, we present our central analysis showing positive graph curvature is associated with over-smoothing, while negative graph curvature is associated with over-squashing. In Section 4, we introduce the novel graph rewiring method BORF, which modifies the local graph geometry to suppress over-smoothing and support over-squashing inducing connections. We empirically demonstrate the superior performance of our method compared to other state-of-the-art rewiring methods in Section 5. Related works are mentioned in passing in Section 6. The paper ends with concluding remarks in Section 7. Technical proofs and other additional materials are provided in the Appendix.

Notation. We denote scalars by lower- or upper-case letters and vectors and matrices by lower- and upper-case boldface letters, respectively. We use $\mathcal{G} = (\mathcal{V}, \mathcal{E})$ to denote a simple, connected graph $\mathcal{G}$ with vertex set $\mathcal{V}$ and edge set $\mathcal{E}$. Graph vertices are also referred to as nodes, and the characters u, v, w, p, q are reserved for representing them. We write $u \sim v$ if $(u, v) \in \mathcal{E}$. The shortest path distance between two vertices u, v is denoted by $d(u, v)$. We let $\mathcal{N}_u = \{p \in \mathcal{V} \mid p \sim u\}$ be the 1-hop neighborhood and $\tilde{\mathcal{N}_u} = \mathcal{N}_u \cup \{u\}$ be the extended neighborhood of u.

2. Preliminaries

We begin by summarizing the relevant backgrounds on message passing neural networks (MPNN) and the over-smoothing and over-squashing issues of GNNs. We also provide a concise formulation for the Ollivier-Ricci curvature on graphs.

2.1. Message Passing Neural Networks

Message passing neural networks (MPNNs) (Gilmer et al., 2017) is a unified framework for a broad range of graph neural networks. It encompasses virtually every popular GNN design to date, including graph convolutional network (GCN) (Kipf & Welling, 2017), GraphSAGE (Hamilton et al., 2017), graph attention network (GAT) (Veličković et al., 2018), graph isomorphism network (GIN) (Xu et al., 2019), etc. The key idea behind MPNNs is that by aggregating information from local neighborhoods, a neural network can effectively use both node feature data and the graph topology to learn relevant information.

Let $\boldsymbol{X} \in \mathbb{R}^{|\mathcal{V}| \times d}$ be the node feature matrix of a graph $\mathcal{G}$, where d is the number of feature channels. Let $\boldsymbol{X}^k$ be the node feature matrix at layer k, with the convention that $\boldsymbol{X}^0 = \boldsymbol{X}$. The features of node u at layer k is denoted by $\boldsymbol{X}_u^k$, and is exactly the transpose of the u-th row of $\boldsymbol{X}^k$. A general formulation for an MPNN can be given by

$$\boldsymbol{X}_u^{k+1} = \phi_k\left(\bigoplus_{p \in \tilde{\mathcal{N}_u}} \psi_k(\boldsymbol{X}_p^k)\right), \tag{1}$$

where ψ_k is a message function, $\bigoplus$ is an aggregating function, and ϕ_k is an update function. Table 1 summarizes the choice for ψ_k, ϕ_k, and $\bigoplus$ in four popular GNN architectures. We give further discussion on how Equation (1) accommodates different designs of GNNs in Appendix A. From now on, we will use MPNN and GNN interchangeably.

Table 1. Popular GNNs are instances of Equation (1): GCN (Kipf & Welling, 2017), GraphSAGE (Hamilton et al., 2017), GAT (Veličković et al., 2018), and GIN (Xu et al., 2019).

GNN	ψ_k	ϕ_k	$\bigoplus$
GCN [1]	linear	activation	mean
GraphSAGE [2]	linear	activation	mean
GAT	linear	activation	weighted mean
GIN [3]	identity	MLP	sum

Traditionally, GNNs are designed to operate directly on the input graphs. In many cases, this leads to significant downsides due to possible undesirable characteristics of the dataset. Hence, it has been proposed that by conducting the learning process on a modified version of the input graphs, we can improve upon the scale and performance of graph models (Hamilton et al., 2017; Gasteiger et al., 2019). One such approach is known as graph rewiring, which involves adding or modifying the set of edges $\mathcal{E}$ within a graph as a preprocessing step. We give a brief overview of two novel rewiring algorithms, SDRF (Topping et al., 2022) and FoSR (Karhadkar et al., 2023), along with a comparison between them and our proposed method in Section 4.

[1] If the symmetrically normalized Laplacian is replaced by the normalized Laplacian. See Appendix A.

[2] Mean aggregator variant.

[3] GIN-0 variant.

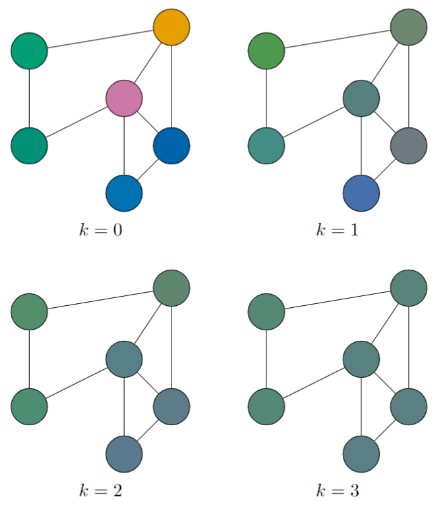

Figure 1. Over-smoothing induced by the averaging operation.

2.2. The Over-smoothing and Over-squashing Issues of GNNs

Over-smoothing has generally been described as the phenomenon where the feature representation of every node becomes similar to each other as the number of layers in a GNN increases (Li et al., 2018a). If over-smoothing occurs, for every two neighbor nodes u, v, it must happen that

$$\left|\boldsymbol{X}_u^k - \boldsymbol{X}_v^k\right| \to 0 \text{ as } k \to \infty. \tag{2}$$

Equation 2 can be thought of as the local smoothing behavior, observed in the neighborhood of two nodes $u \sim v$.

A global formulation for feature representation similarity is obtained by summing up terms of the form $\left|\boldsymbol{X}_u^k - \boldsymbol{X}_v^k\right|$ for all neighbors u, v. Formally, we yield a formulation for the global over-smoothing issue based on local observations

$$\sum_{(u,v)\in\mathcal{E}} \left|\boldsymbol{X}_u^k - \boldsymbol{X}_v^k\right| \to 0 \text{ as } k \to \infty. \tag{3}$$

That is, if the term $\sum_{(u,v)\in\mathcal{E}} \left|\boldsymbol{X}_u^k - \boldsymbol{X}_v^k\right|$ converges to zero, we say that the model experiences over-smoothing. This definition is similar to the one introduced in (Rusch et al., 2022). Figure 1 visualizes the over-smoothing behavior of a simple 6-node graph with RGB color features. At the start, the nodes can be roughly divided into 4 classes: green, blue, yellow, and pink. When smoothing by the mean operation is applied repeatedly for k times, different nodes rapidly converge to having similar colors. At the final step $k = 3$, nodes have become virtually indistinguishable - they experienced over-smoothing.

On the other hand, over-squashing is an inherent pitfall of GNNs that occurs when bottlenecks in the graph structure impede the graph's ability to propagate information among its vertices. We observe from Equation 1 that messages can only be transmitted by a distance of 1 at each layer. Hence, two nodes of distance K will only receive information from each other if the GNN has at least K layer. However, as the number of layers increases, the size of each node's receptive field increases exponentially (Chen et al., 2018a). This causes messages between exponentially-growing number of distant vertices to be squashed into fixed size vectors, limiting the model's ability to capture long range dependencies (Alon & Yahav, 2021). As illustrated in Figure 2, graph bottlenecks contribute to this problem by enforcing the maximal rate of expansion to the receptive field, while providing minimal connection between either sides of the bottleneck. Thus, a graph containing many bottlenecks is likely to suffer from over-squashing.

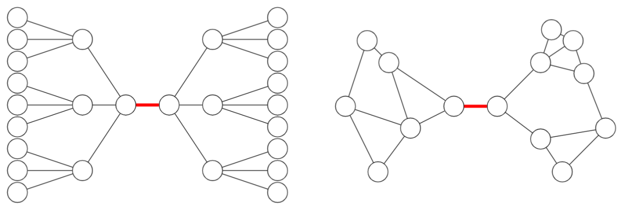

Figure 2. Bottlenecks (colored in red) inhibit the message passing capability of MPNNs.

We remark that over-squashing is a relatively novel observation, and an appropriate way to formulate it is currently lacking from the literature (see Appendix B).

2.3. Ollivier-Ricci Curvature on Graph

The Ricci curvature is a geometric object ubiquitous in the field of differential geometry. At a local neighborhood of a Riemannian manifold, the Ricci curvature of the space characterizes the average geodesic dispersion, i.e., whether straight paths in a given direction of nearby points have the tendency to remain parallel (zero curvature), converge (positive curvature), or diverge (negative curvature). Crucially, the definition of the Ricci curvature depends on the ability to specify directions, or more precisely, tangent vectors, within the space considered.

To circumvent the lack of a tangent structure on graphs, the Ollivier-Ricci curvature (Ollivier, 2009) considers random walkers from nearby points. We define a random walk m on a graph $\mathcal{G}$ as a family of probability measure $m_u(\cdot)$ on $\mathcal{V}$ for all $u \in \mathcal{V}$. For $p \in \mathcal{V}$, it is intuitive to think of $m_u(p)$ as the probability that a random walker starting from u will end up at p. Then, for any $u, v \in \mathcal{V}$, we can consider the L^1 Wasserstein transport distance $W_1(m_u, m_v)$ given by

$$W_1(m_u, m_v) = \inf_{\pi\in\Pi(m_u,m_v)} \left(\sum_{(p,q)\in\mathcal{V}^2} \pi(p,q)d(p,q) \right),$$

where $\Pi(m_u, m_v)$ is the family of joint probability distributions of m_u and m_v. This measures the minimal distance that random walkers from u must travel to meet the random walkers from v. The Ollivier-Ricci curvature $\kappa(u,v)$ is then defined based on the ratio between the random walker distance $W_1(m_u, m_v)$ and the original distance $d(u,v)$

$$\kappa(u,v) = 1 - \frac{W_1(m_u, m_v)}{d(u,v)}. \tag{4}$$

Such definition captures the behavior that $\kappa(u,v) = 0$ if the random walkers have a tendency to remain at equal distance, $\kappa(u,v) < 0$ if the random walkers diverge, and $\kappa(u,v) > 0$ if the random walkers converge.

On simple graphs, it is natural to consider the uniform random walk m given by

$$m_u(p) = \begin{cases} \frac{1}{\deg u} & \text{if } p \sim u, \\ 0 & \text{otherwise.} \end{cases}$$

Hence, the Ollivier-Ricci curvature on graphs κ is defined by Equation 4, where $W_1(m_u, m_v)$ is the optimal value of the objective function in the linear optimization problem

$$\begin{aligned} \text{minimize} \quad & \sum_{p \in \mathcal{N}_u} \sum_{q \in \mathcal{N}_v} d(p,q)\pi(p,q) \\ \text{subject to} \quad & \sum_{p \in \mathcal{N}_u} \pi(p,q) = \tfrac{1}{\deg v}, \\ & \sum_{q \in \mathcal{N}_v} \pi(p,q) = \tfrac{1}{\deg u}. \end{aligned} \tag{5}$$

3. Analysis Based on Graph Curvature

Since curvature is inherently a local notion, it makes sense to restrict our attention to nodes of distance 1. Throughout this section, unless otherwise stated, we assume $u \sim v \in \mathcal{V}$ are neighboring vertices with $\deg u = n, \deg v = m$, and $n \geq m$. We note from Equation 4 that the bound

$$-2 \leq \kappa(u,v) \leq 1$$

is always satisfied, and so a curvature value close to 1 is considered very positive, while a value close to -2 is considered very negative.

To motivate our findings, we remark that the curvature $\kappa(u,v)$ characterizes how well-connected the neighborhoods $\tilde{\mathcal{N}}(u)$ and $\tilde{\mathcal{N}}(v)$ are. Figure 3 illustrates how different local graph structures give rise to different graph curvature. Red and blue are used to color the neighborhoods $\tilde{\mathcal{N}}_u \backslash \{v\}$ and $\tilde{\mathcal{N}}_v \backslash \{u\}$. The color violet is used to signal shared vertices or edges connecting from one neighborhood to the other. If the neighborhoods mostly coincide then the transport cost is very low, leading to a positive curvature value. In this case, messages can be transmitted freely and

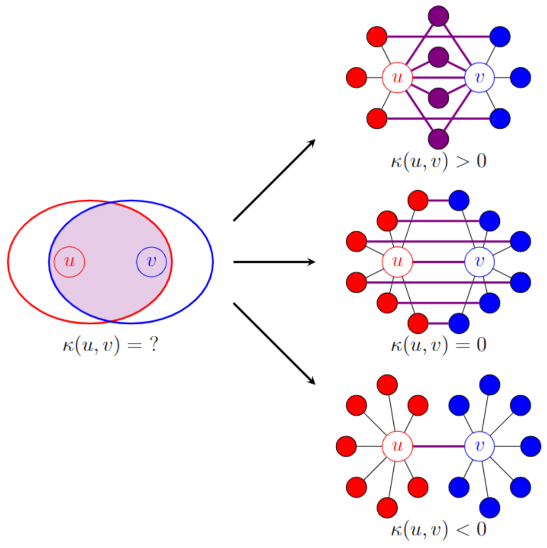

Figure 3. Different edge curvatures give rise to different local graph structures.

easily between both neighborhoods. In contrast, if the neighborhoods only have minimal connections then the transport cost is high, leading to a negative curvature value. Each such connection will then act as a bottleneck, limiting the effectiveness of the message-passing mechanism.

3.1. Positive Graph Curvature and Over-smoothing

We identify the key connection between positive graph curvature and the occurrence of the over-smoothing issue.

Lemma 3.1. *The following inequality holds*

$$\frac{|\mathcal{N}_u \cap \mathcal{N}_v|}{\max(m,n)} \geq \kappa(u,v).$$

Lemma 3.1 says that the curvature $\kappa(u,v)$ is a lower bound for the proportion of shared neighbors between u and v. A closer inspection of Equation (1) reveals a fundamental characteristic of GNNs: at the k-th layer, every node p broadcasts an identical message $\psi_k(\boldsymbol{X}_p^k)$ to each vertex u in its 1-hop neighborhood. These messages are then aggregated and used to update the features of u. If $\kappa(u,v)$ is very positive then the neighborhoods $\mathcal{N}_u$ and $\mathcal{N}_v$ mostly coincides. Hence, they incorporate roughly the same information, and their variance diminishes. This gives us significant insight into why over-smoothing happens, and is made precise by the following theorem.

Theorem 3.2. *Consider the update rule given by Equation (1). Suppose the edge curvature $\kappa(u,v) > 0$. For some k, assume the update function ϕ_k is L-Lipschitz, $|\boldsymbol{X}_p^k| \leq C$ for all $p \in \mathcal{N}(u) \cup \mathcal{N}(v)$, and the message function ψ_k is bounded, i.e. $|\psi_k(\boldsymbol{x})| \leq M|\boldsymbol{x}|, \forall \boldsymbol{x}$. There exists a positive function $h : (0,1) \to \mathbb{R}^+$ dependent on the constants L, M, C, n satisfying*

- *if $\bigoplus$ is the sum operation then h is constant;*
- *if $\bigoplus$ is the mean operation then h is decreasing;*

such that

$$\left|\boldsymbol{X}_u^{k+1} - \boldsymbol{X}_v^{k+1}\right| \leq (1-\kappa(u,v))h(\kappa(u,v)). \quad (6)$$

In both cases, we clearly have

$$\lim_{x\to 1}(1-x)h(x) = 0. \quad (7)$$

This result applies to a wide range of GNNs, including those in Table 1 with the exception of GAT, due to the fact that GAT employs the attention mechanism to create a learnable weighted mean function as the aggregator. Nevertheless, if the variance between attention weights are low, we expect the general behavior to still hold true.

Theorem 3.2 conclusively shows that locally, very positively curved edges force node features to become similar. If the graph is very positively curved everywhere, or if it contains multiple subgraphs with such characteristic, we can expect the features of all nodes to converge to indistinguishable representations. This is exactly the mixing behavior observed by Li et al. (2018a), suggesting that the occurrence of over-smoothing can be explained by an overly abundance number of edges with positive graph curvature.

Any global analysis of the issue based on local observations is hindered by the complexity in dealing with graph structures. Nevertheless, by restricting our attention to a more manageable class of graphs - the class of regular graphs, we obtain Proposition 3.3. This serves to illustrate how positive local graph curvature can affect the long term global behavior of a typical GNN.

Proposition 3.3. *Assume the graph is regular. Suppose there exists a constant $\delta > 0$ such that for all edges $(u,v) \in \mathcal{E}$, the curvature is bounded by $\kappa(u,v) \geq \delta > 0$. Consider the update rule given by equation 1. For all $k \geq 1$, assume the functions ϕ_k are L-Lipschitz, $\bigoplus$ is realised as the mean operation, $\left|\boldsymbol{X}_p^0\right| \leq C$ for all $p \in \mathcal{V}$, and the functions ψ_k are bounded linear operators, i.e. $|\psi_k(\boldsymbol{x})| \leq M|\boldsymbol{x}|, \forall \boldsymbol{x}$. The following inequality holds for $k \geq 1$ and any neighboring vertices $u \sim v$*

$$\left|\boldsymbol{X}_u^k - \boldsymbol{X}_v^k\right| \leq \frac{2}{3}C\left(\frac{3LM\lfloor(1-\delta)n\rfloor}{n+1}\right)^k. \quad (8)$$

Furthermore, for any $u, v \in \mathcal{V}$ that are not necessarily neighbors, the following inequality holds

$$\left|\boldsymbol{X}_u^k - \boldsymbol{X}_v^k\right| \leq \frac{2}{3}\left\lfloor\frac{2}{\delta}\right\rfloor C\left(\frac{3LM\lfloor(1-\delta)n\rfloor}{n+1}\right)^k. \quad (9)$$

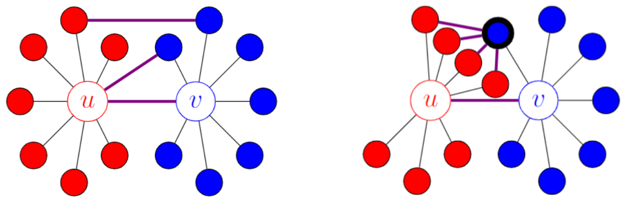

(a) Violet edges connecting $\tilde{\mathcal{N}}_u\backslash\{v\}$ and $\tilde{\mathcal{N}}_v\backslash\{u\}$ serve as information pathways.

(b) Edges may exacerbate the situation by creating new bottlenecks.

Figure 4. Identifying connections that enable effective message-passing at local neighborhoods.

The conclusion of Proposition 3.3 says that if every edge curvature in a regular graph G is bounded from below by a sufficiently high constant δ then the difference between the features of any pair of neighboring nodes, or indeed, any pair of nodes at all, exponentially converges to 0 in a typical GNN. This leads to the over-smoothing issue formulated in Equation (3) since for appropriate constants $C_1, C_2 > 0$, we have

$$\sum_{(u,v)\in\mathcal{E}} \left|\boldsymbol{X}_u^k - \boldsymbol{X}_v^k\right| \leq C_1 e^{-C_2 k}.$$

In real world graphs, it is often the case that not all edges in a graph are positively curved. Nevertheless, we expect an abundance of edges with overly high curvature will either cause or worsen the over-smoothing issue in GNNs.

3.2. Negative Graph Curvature and Over-squashing

In this section, we demonstrate the intimate connection between negative graph curvature and the occurrence of local bottlenecks, which in turn causes over-squashing.

Message-passing across local neighborhoods is facilitated by connections of the form (p,q) with $p \in \tilde{\mathcal{N}}_u\backslash\{v\}$ and $q \in \tilde{\mathcal{N}}_v\backslash\{u\}$. As visualized by Figure 4a, such edges (colored in violet) provide information pathways between $\tilde{\mathcal{N}}_u$ and $\tilde{\mathcal{N}}_v$. However, a large number of these edges concentrated on a relatively few vertices will create new bottlenecks, instead of providing good message channels. Figure 4b illustrates this point, as there are way too many edges connecting to the emphasized node but too little edges connecting between other neighbors. Since $n \geq m$, there is a natural squashing of information as messages are transmitted from $\mathcal{N}_u$ to $\mathcal{N}_v$ of ratio $\frac{n}{m}$. We identify the edges that provide good pathways as those that do not exacerbate this ratio and restrict our attention to these edges.

We characterize the effect of edge curvature on graph bottlenecks in the following proposition.

Proposition 3.4. *Let $\tilde{\mathcal{E}}$ be union of the edge set $\mathcal{E}$ with the set of all possible self-loops. Let S be the subset of $\tilde{\mathcal{E}}$*

containing edges of the form (p,q) with $p \in \tilde{\mathcal{N}}_u \backslash \{v\}$ and $q \in \tilde{\mathcal{N}}_v \backslash \{u\}$. Supposing each vertex w is a vertex of at most $\frac{n}{m}$ edges in S. The following inequality holds

$$|S| \leq \frac{n(\kappa(u,v)+2)}{2}. \tag{10}$$

Recall that the curvature is deemed very negative if it is close to -2. Proposition 3.4 shows that very negative edge curvature values prohibit the number of information pathways from $\tilde{\mathcal{N}}_u$ to $\tilde{\mathcal{N}}_v$, and very negatively curved edges induce local bottlenecks. This in turn contributes to the occurrence of the over-squashing issue as proposed by Alon & Yahav (2021). We note that an adequate measure for the over-squashing issue is currently lacking in the literature (see Appendix B). Inspired by the influence distribution introduced by Xu et al. (2018), the next theorem asserts that negative edge curvature directly causes the decaying importance of distant nodes in GNNs with non-linearity removed. This demonstrates the effect of edge curvature on the over-squashing issue.

Theorem 3.5. *Consider the update rule given by Equation (1). Suppose ψ_k, ϕ_k are linear operators for all k, and $\bigoplus$ is the sum operation. If u, v are neighboring vertices with neighborhoods as in Proposition 3.4 and S is defined similarly then for all $p \in \tilde{\mathcal{N}}_u \backslash \{v\}$, $q \in \tilde{\mathcal{N}}_v \backslash \{u\}$, we have*

$$\begin{aligned} \left[\frac{\partial \boldsymbol{X}_u^{k+2}}{\partial \boldsymbol{X}_q^k}\right] &= \alpha \sum_{w \in V} \left[\frac{\partial \boldsymbol{X}_u^{k+2}}{\partial \boldsymbol{X}_w^k}\right], \\ \left[\frac{\partial \boldsymbol{X}_v^{k+2}}{\partial \boldsymbol{X}_p^k}\right] &= \beta \sum_{w \in V} \left[\frac{\partial \boldsymbol{X}_v^{k+2}}{\partial \boldsymbol{X}_w^k}\right], \end{aligned} \tag{11}$$

where $\left[\frac{\boldsymbol{y}}{\boldsymbol{x}}\right]$ is used to denote the Jacobian of $\boldsymbol{y}$ with regard to $\boldsymbol{x}$, and α, β satisfy

$$\begin{aligned} \alpha &\leq \frac{|S|+2}{\sum_{w \in \tilde{\mathcal{N}}_v} (\deg(w)+1)}, \\ \beta &\leq \frac{|S|+2}{\sum_{w \in \tilde{\mathcal{N}}_u} (\deg(w)+1)}. \end{aligned} \tag{12}$$

To understand the meaning of Theorem 3.5, let us fix $k = 0$ and assume $\mathcal{G}$ is a regular graph with node degree n. Equations (11) and (12), along with Proposition 3.4, say that the contribution by the vertex q to the vertex u relative to the contribution of all other vertices, measured by the scaling term α in regard to the Jacobians, is bounded by

$$\alpha \leq \frac{n(\kappa(u,v)+2)+4}{2(n+1)^2}.$$

Hence, if $\kappa(u,v)$ is very negative and n is large, we expect that the messages from each node of $\mathcal{N}_v$ make up only $\frac{2}{(n+1)^2}$ of the total sum of information. They thus hardly have any effect on u, even when the distance between them is only 2. An analogous result holds for the case when $\bigoplus$ is the mean operation without much modification.

Algorithm 1 Batch Ollivier-Ricci Flow (BORF)

```
Input: graph $\mathcal{G} = (\mathcal{V}, \mathcal{E})$, # rewiring batches $n$, # edges
added per batch $h$, # edges removed per batch $k$
for $i = 1$ to $n$ do
  Find $h$ edges $(u_1, v_1), \ldots, (u_h, v_h)$ with minimal
  Ollivier-Ricci curvature $\kappa$, along with each summand
  $\pi_j(p,q)d(p,q)$ in their optimal transportation cost sum
  for all $p, q \in \mathcal{V}$ and $j = \overline{1,h}$
  Find $k$ edges $(u^1, v^1), \ldots, (u^k, v^k)$ with maximal
  Ollivier-Ricci curvature $\kappa$
  for $j = 1$ to $h$ do
    Add to $\mathcal{G}$ the edge $(p^*, q^*)$ given by
        $(p^*, q^*) = \operatorname{argmax} d(p,q)\pi_j(p,q)$
  end for
  Remove edges $(u^1, v^1), \ldots, (u^k, v^k)$ from $\mathcal{G}$
end for
```

We have thus shown that negative curvature characterizes graph bottlenecks. As such, GNNs that operate on graphs with a large volume of negatively curved edges are expected to suffer from over-squashing.

4. BORF: Batch Ollivier-Ricci Flow

Our theoretical results reveal the strikingly simple geometric connection between the over-smoothing and over-squashing issues: over-smoothing happens when there is a large proportion of edges with very positive curvature, while over-squashing occurs when there is a large proportion of edges with very negative curvature. As a natural extension, we propose the Batch Ollivier-Ricci Flow (BORF), a graph rewiring algorithm capable of simultaneously mitigating these issues by suppressing the over-smoothing and supporting the over-squashing inducing graph edges (see Algorithm 1).

For each of n batches, BORF first finds the h edges $(u_1, v_1), \ldots, (u_h, v_h)$ with minimal curvature and k edges $(u^1, v^1), \ldots, (u^k, v^k)$ with maximal curvature within the graph. Then, it tries to uniformly alleviate graph bottlenecks by adding connections to the set of h minimally curved edges. To save on computation time, BORF does not recalculate the graph curvature within each batch. Instead, for each edge with minimal curvature (u_j, v_j), it reuses the already calculated optimal transport plan π_j between m_{u_j} and m_{v_j} to decide which edge should be added. Recall that the formula for the optimal transport cost is

$$W_1(m_{u_j}, m_{v_j}) = \sum_{(p,q)} \pi_j(p,q) d(p,q).$$

Hence, to minimize the transport cost, it makes sense to rewire the two nodes that contribute the most to this sum. Specifically, we choose to add to $\mathcal{G}$ the edge (p^*, q^*) such that

$$(p^*, q^*) = \operatorname{argmax} d(p,q)\pi_j(p,q).$$

If there are multiple candidates, we arbitrarily choose one. Finally, BORF removes the k maximally curved edges $(u^1, v^1), \ldots, (u^k, v^k)$ whose presence might prime the over-smoothing behavior to occur.

With such design, BORF can effectively limit both ends of the curvature spectrum, simultaneously suppressing over-smoothing and supporting over-squashing inducing connections. Furthermore, depending on data characteristics, we may change the behaviours of BORF to either be a net edge add, net edge minus, or net zero rewiring algorithm. Thereby, BORF permits fine-tuned and fluid adjustments of the total number of edges and their curvature range.

Other rewiring algorithms. SDRF (Topping et al., 2022) and FoSR (Karhadkar et al., 2023) are state-of-the-art rewiring algorithms for GNNs, designed with the purpose of alleviating the over-squashing issue. SDRF is based on the edge metric Balanced Forman curvature (BFC), which is actually a lower bound for the Ollivier-Ricci curvature. At its core, SDRF iteratively finds the edge with the lowest BFC, calculate the change in BFC for every possible edge that can be added, then add the one edge that affects the greatest change to the BFC of the aforementioned edge. On the other hand, FoSR is based on the heuristics that the spectral gap characterizes the connectivity of a graph. At each step, it approximates which missing edge would maximally improve the spectral gap and add that edge to the graph.

Comparision to SDRF. BORF shares some similarities to SDRF, but with notable differences. Since SDRF is based on BFC, it can only accurately enforce a lower bound on the Ollivier-Ricci curvature. Furthermore, its design lacks the capability to be used as a net edge minus rewiring algorithm. As such, it is ill-equipped to deal with the over-smoothing issue or to be used on denser graphs. Another difference is BORF calculates the graph curvature very infrequently, while SDRF has to constantly recalculate for each possible new edge. Finally, by rewiring edges in batch, BORF affects a uniform change across the graph. This helps to preserve the graph topology and prevent the possibility that a small outlier subgraph gets continually rewired, while other parts of the graph do not see any geometrical improvement.

Comparision to FoSR. Unlike BORF and SDRF, FoSR does not have the ability to remove edges. Hence, despite over-smoothing and over-squashing being problems on the two ends of the same spectrum, the algorithm is incapable of addressing the first issue. It is also very challenging to predict where new edges will be added and what changes FoSR would make to the graph topology. This might complicate attempts by users to analyse the performance changes made by the algorithm.

5. Experiments

In this section, we empirically verify the effectiveness of BORF on a variety of tasks compared to other rewiring alternatives. We seek to demonstrate the potential of curvature-based rewiring methods, and more generally, geometric-aware techniques in improving the performance of GNNs.

Datasets. We conduct our experiments on a range of widely used node classification and graph classification tasks. For node classification, we report our results on the datasets CORA, CITESEER (Yang et al., 2016), TEXAS, CORNELL, WISCONSIN (Pei et al., 2020) and CHAMELEON (Rozemberczki et al., 2019). For graph classification, we validate our method on the following benchmarks: ENZYMES, IMDB, MUTAG and PROTEINS from the TUDataset (Morris et al., 2020). A summary of dataset statistics is available in Appendix E.

Experiment details. We chose to compare BORF to no graph rewiring and two other state-of-the-art rewiring methods: SDRF (Topping et al., 2022) and FoSR (Karhadkar et al., 2023). We applied each method as a preprocessing step to all graphs in the datasets considered, before feeding the rewired graph data into a GNN to evaluate performance. For baseline GNNs, we employed the popular graph architectures GCN (Kipf & Welling, 2017) and GIN (Xu et al., 2019). For each task and baseline model, we used the same settings of GNN and optimization hyper-parameters across all rewiring methods to rule out hyper-parameter tuning as a source of performance gain. The setting for each rewiring option was obtained by tuning every hyper-parameter available for each method with the exception of the temperature τ of SDRF, which we set to ∞. Each configuration is evaluated using the validation set. The test set accuracy of the configuration with the best validation performance is then recorded. For each experiment, we accumulate the result across 100 random trials and report the mean test accuracy, along with the 95% confidence interval. Further experiment details are available in Appendix D.

Results. Table 2 and Table 3 summarize our experiment results for node classification and graph classification datasets, respectively. BORF outperforms all other methods in every node classification tasks on both GCN and GIN. It is worth mentioning that the 95% confidence interval of BORF is almost always smaller than other methods, indicating a con-

Table 2. Classification accuracies of GCN and GIN with None, SDRF, FoSR, and BORF rewiring on various node classification datasets. Best results are highlighted in bold.

	GCN				GIN			
DATA SET	NONE	SDRF	FOSR	BORF	NONE	SDRF	FOSR	BORF
CORA	86.7 ± 0.3	86.3 ± 0.3	85.9 ± 0.3	$\mathbf{87.5 \pm 0.2}$	76.0 ± 0.6	74.9 ± 0.1	75.1 ± 0.8	$\mathbf{78.4 \pm 0.4}$
CITESEER	72.3 ± 0.3	72.6 ± 0.3	72.3 ± 0.3	$\mathbf{73.8 \pm 0.2}$	59.3 ± 0.9	60.3 ± 0.8	61.7 ± 0.7	$\mathbf{63.1 \pm 0.8}$
TEXAS	44.2 ± 1.5	43.9 ± 1.6	46.0 ± 1.6	$\mathbf{49.4 \pm 1.2}$	53.5 ± 3.1	50.3 ± 3.7	47.0 ± 3.7	$\mathbf{63.1 \pm 1.7}$
CORNELL	41.5 ± 1.8	42.2 ± 1.5	40.2 ± 1.6	$\mathbf{50.8 \pm 1.1}$	36.5 ± 2.2	40.0 ± 2.1	35.6 ± 2.4	$\mathbf{48.6 \pm 1.2}$
WISCONSIN	44.6 ± 1.4	46.2 ± 1.2	48.3 ± 1.3	$\mathbf{50.3 \pm 0.9}$	48.5 ± 2.2	48.8 ± 1.9	48.5 ± 2.1	$\mathbf{54.9 \pm 1.2}$
CHAMELEON	59.2 ± 0.6	59.4 ± 0.5	59.3 ± 0.6	$\mathbf{61.5 \pm 0.4}$	58.1 ± 2.1	58.4 ± 2.1	56.3 ± 2.2	$\mathbf{65.3 \pm 0.8}$

Table 3. Classification accuracies of GCN and GIN with None, SDRF, FoSR, and BORF rewiring on various graph classification datasets. Best results are highlighted in bold.

	GCN				GIN			
DATA SET	NONE	SDRF	FOSR	BORF	NONE	SDRF	FOSR	BORF
ENZYMES	25.5 ± 1.3	26.1 ± 1.1	$\mathbf{27.4 \pm 1.1}$	24.7 ± 1.0	31.3 ± 1.2	33.5 ± 1.3	25.3 ± 1.2	$\mathbf{35.5 \pm 1.2}$
IMDB	49.3 ± 1.0	49.1 ± 0.9	49.6 ± 0.8	$\mathbf{50.1 \pm 0.9}$	69.0 ± 1.3	68.6 ± 1.2	69.5 ± 1.1	$\mathbf{71.3 \pm 1.5}$
MUTAG	68.8 ± 2.1	70.5 ± 2.1	75.6 ± 1.7	$\mathbf{75.8 \pm 1.9}$	75.5 ± 2.9	77.3 ± 2.3	75.2 ± 3.0	$\mathbf{80.8 \pm 2.5}$
PROTEINS	70.6 ± 1.0	71.4 ± 0.8	$\mathbf{72.3 \pm 0.9}$	71.0 ± 0.8	69.7 ± 1.0	72.2 ± 0.9	$\mathbf{74.2 \pm 0.8}$	71.3 ± 1.0

sistent level of performance. This result agrees with what is expected since SDRF and FoSR are not suited for dealing with the over-smoothing issue, which heavily degrades the model's performance on node classification tasks. On graph classification datasets, BORF achieves higher test accuracy compared to other rewiring options in most settings.

6. Related Work

Over-smoothing: First recognised by Li et al. (2018a), who observed that GCN with non-linearity removed induces a smoothing effect on data features, over-smoothing has been one of the focal considerations in the study of GNNs. A dynamical system approach was used by Oono & Suzuki (2020) to show that under considerable assumptions, even GCN with ReLU can not escape this plight. Follow-up work by Cai & Wang (2020) generalized and improved this approach. Designing ways to alleviate or purposefully avoid the problem is a lively research area (Luan et al., 2019; Zhao & Akoglu, 2020; Rusch et al., 2022). Notably, randomly removing edges from the base graph consistently improves GNN performance (Rong et al., 2020).

Over-squashing: The inability of GNNs to effectively take into account distant information has long been observed (Xu et al., 2018). Alon & Yahav (2021) showed that this phenomenon can be explained by the existence of local bottlenecks in the graph structure. It was suggested by Topping et al. (2022) that graph curvature provides an insightful way to address the over-squashing problem. Methods have been designed to tackle this problem, including those of Banerjee et al. (2022) and Karhadkar et al. (2023).

Graph curvature: Efforts have been made to extend the geometric notion of curvature to settings other than smooth manifolds, including on graphs (Bakry & Émery, 1985; Forman, 2003). Among these, the Ollivier's Ricci curvature (Ollivier, 2009) is arguably the superior attempt due to its proven compatibility with the classical notion of curvature in differential geometry (Lin et al., 2011; van der Hoorn et al., 2020). Graph curvature has been utilised in the study of complex networks (Ni et al., 2015; Sia et al., 2019), and a number of works have experimented with its use in GNNs (Topping et al., 2022; Bober et al., 2022).

7. Conclusion

In this paper, we established the novel correspondence between the Ollivier-Ricci curvature on graphs with the over-smoothing and over-squashing issues. In specific, we showed that positive graph curvature is associated with over-smoothing, while negative graph curvature is associated with over-squashing. Based on our theoretical results, we proposed Batch Ollivier-Ricci Flow, a novel curvature based rewiring method that can effectively improve GNN performance by tackling both the over-smoothing and over-squashing problems at the same time. It is interesting to note that by different definitions of the random walk m_u, we may be able to capture different behaviors of the local graph structures using graph curvature. To lower computational cost and speed up run time, we may also consider replacing the optimal transport implementation of BORF by the sliced optimal transport. We leave studying such modifications as directions for future work.

References

Alon, U. and Yahav, E. On the bottleneck of graph neural networks and its practical implications. In *International Conference on Learning Representations*, 2021. URL https://openreview.net/forum?id=i80OPhOCVH2.

Bakry, D. and Émery, M. Diffusions hypercontractives. In Azéma, J. and Yor, M. (eds.), *Séminaire de Probabilités XIX 1983/84*, pp. 177–206, Berlin, Heidelberg, 1985. Springer Berlin Heidelberg. ISBN 978-3-540-39397-9.

Banerjee, P. K., Karhadkar, K., Wang, Y. G., Alon, U., and Montúfar, G. Oversquashing in GNNs through the lens of information contraction and graph expansion. In *2022 58th Annual Allerton Conference on Communication, Control, and Computing (Allerton)*, pp. 1–8, 2022.

Battaglia, P., Pascanu, R., Lai, M., Jimenez Rezende, D., et al. Interaction networks for learning about objects, relations and physics. *Advances in neural information processing systems*, 29, 2016.

Berg, R. v. d., Kipf, T. N., and Welling, M. Graph convolutional matrix completion, 2017. URL https://arxiv.org/abs/1706.02263.

Bober, J., Monod, A., Saucan, E., and Webster, K. N. Rewiring networks for graph neural network training using discrete geometry, 2022. URL https://arxiv.org/abs/2207.08026.

Bojchevski, A., Shchur, O., Zügner, D., and Günnemann, S. Netgan: Generating graphs via random walks. In *International conference on machine learning*, pp. 610–619. PMLR, 2018.

Bourne, D., Cushing, D., Liu, S., Münch, F., and Peyerimhoff, N. Ollivier–ricci idleness functions of graphs. *SIAM Journal on Discrete Mathematics*, 32, 04 2017. doi: 10.1137/17M1134469.

Bronstein, M. M., Bruna, J., Cohen, T., and Veličković, P. Geometric deep learning: Grids, groups, graphs, geodesics, and gauges, 2021. URL https://arxiv.org/abs/2104.13478.

Cai, C. and Wang, Y. A note on over-smoothing for graph neural networks, 2020. URL https://arxiv.org/abs/2006.13318.

Chen, J., Zhu, J., and Song, L. Stochastic training of graph convolutional networks with variance reduction. In *International Conference on Machine Learning*, pp. 941–949, 2018a.

Chen, Y., Wei, Z., and Huang, X. Incorporating corporation relationship via graph convolutional neural networks for stock price prediction. In *Proceedings of the 27th ACM International Conference on Information and Knowledge Management*, CIKM '18, pp. 1655–1658, New York, NY, USA, 2018b. Association for Computing Machinery. ISBN 9781450360142. doi: 10.1145/3269206.3269269. URL https://doi.org/10.1145/3269206.3269269.

Duvenaud, D. K., Maclaurin, D., Iparraguirre, J., Bombarell, R., Hirzel, T., Aspuru-Guzik, A., and Adams, R. P. Convolutional networks on graphs for learning molecular fingerprints. *Advances in neural information processing systems*, 28, 2015.

Estrada, E. and Bonchev, D. *Chemical Graph Theory*, pp. 1538–1558. 12 2013. ISBN ISBN 9781439880180. doi: 10.1201/b16132-92.

Fan, W., Ma, Y., Li, Q., He, Y., Zhao, E., Tang, J., and Yin, D. Graph neural networks for social recommendation. In *The World Wide Web Conference*, WWW '19, pp. 417–426, New York, NY, USA, 2019. Association for Computing Machinery. ISBN 9781450366748. doi: 10.1145/3308558.3313488. URL https://doi.org/10.1145/3308558.3313488.

Forman. Bochner's method for cell complexes and combinatorial ricci curvature. *Discrete & Computational Geometry*, 29(3):323–374, Feb 2003. ISSN 1432-0444. doi: 10.1007/s00454-002-0743-x. URL https://doi.org/10.1007/s00454-002-0743-x.

Gasteiger, J., Weißenberger, S., and Günnemann, S. Diffusion improves graph learning, 2019. URL https://arxiv.org/abs/1911.05485.

Gilmer, J., Schoenholz, S. S., Riley, P. F., Vinyals, O., and Dahl, G. E. Neural message passing for quantum chemistry. In *Proceedings of the 34th International Conference on Machine Learning - Volume 70*, ICML'17, pp. 1263–1272. JMLR.org, 2017.

Hamilton, W. L., Ying, R., and Leskovec, J. Inductive representation learning on large graphs. In *Proceedings of the 31st International Conference on Neural Information Processing Systems*, NIPS'17, pp. 1025–1035, Red Hook, NY, USA, 2017. Curran Associates Inc. ISBN 9781510860964.

Harary, F. *Graph Theory and Theoretical Physics*. Academic P., 1967.

Hsu, L. and Lin, C. *Graph Theory and Interconnection Networks*. CRC Press, 2008. ISBN 9781420044829.

Karhadkar, K., Banerjee, P. K., and Montúfar, G. FoSR: First-order spectral rewiring for addressing oversquashing in GNNs. In *International Conference on Learning Representations (ICLR)*, 2023.

Kipf, T., Fetaya, E., Wang, K.-C., Welling, M., and Zemel, R. Neural relational inference for interacting systems. In Dy, J. and Krause, A. (eds.), *Proceedings of the 35th International Conference on Machine Learning*, volume 80 of *Proceedings of Machine Learning Research*, pp. 2688–2697. PMLR, 10–15 Jul 2018. URL https://proceedings.mlr.press/v80/kipf18a.html.

Kipf, T. N. and Welling, M. Semi-Supervised Classification with Graph Convolutional Networks. In *Proceedings of the 5th International Conference on Learning Representations*, ICLR '17, 2017. URL https://openreview.net/forum?id=SJU4ayYgl.

Langley, P. Crafting papers on machine learning. In Langley, P. (ed.), *Proceedings of the 17th International Conference on Machine Learning (ICML 2000)*, pp. 1207–1216, Stanford, CA, 2000. Morgan Kaufmann.

Li, Q., Han, Z., and Wu, X.-M. Deeper insights into graph convolutional networks for semi-supervised learning, 2018a. URL https://arxiv.org/abs/1801.07606.

Li, Y., Vinyals, O., Dyer, C., Pascanu, R., and Battaglia, P. Learning deep generative models of graphs, 2018b.

Lin, Y., Lu, L., and Yau, S.-T. Ricci curvature of graphs. *Tohoku Mathematical Journal*, 63, 12 2011. doi: 10.2748/tmj/1325886283.

Luan, S., Zhao, M., Chang, X.-W., and Precup, D. Break the ceiling: Stronger multi-scale deep graph convolutional networks. In Wallach, H., Larochelle, H., Beygelzimer, A., d'Alché-Buc, F., Fox, E., and Garnett, R. (eds.), *Advances in Neural Information Processing Systems*, volume 32. Curran Associates, Inc., 2019. URL https://proceedings.neurips.cc/paper/2019/file/ccdf3864e2fa9089f9eca4fc7a48ea0a-Paper.pdf.

Matsunaga, D., Suzumura, T., and Takahashi, T. Exploring graph neural networks for stock market predictions with rolling window analysis. *arXiv preprint arXiv:1909.10660*, 2019.

Morris, C., Kriege, N. M., Bause, F., Kersting, K., Mutzel, P., and Neumann, M. Tudataset: A collection of benchmark datasets for learning with graphs, 2020. URL https://arxiv.org/abs/2007.08663.

Ni, C.-C., Lin, Y.-Y., Gao, J., David Gu, X., and Saucan, E. Ricci curvature of the internet topology. In *2015 IEEE Conference on Computer Communications (INFOCOM)*, pp. 2758–2766, 2015. doi: 10.1109/INFOCOM.2015.7218668.

Ollivier, Y. Ricci curvature of markov chains on metric spaces. *Journal of Functional Analysis*, 256(3):810–864, 2009. ISSN 0022-1236. doi: 10.1016/j.jfa.2008.11.001.

Oono, K. and Suzuki, T. Graph neural networks exponentially lose expressive power for node classification. In *International Conference on Learning Representations*, 2020. URL https://openreview.net/forum?id=S1ldO2EFPr.

Paeng, S.-H. Volume and diameter of a graph and ollivier's ricci curvature. *Eur. J. Comb.*, 33:1808–1819, 2012.

Pei, H., Wei, B., Chang, K. C.-C., Lei, Y., and Yang, B. Geom-gcn: Geometric graph convolutional networks, 2020. URL https://arxiv.org/abs/2002.05287.

Rong, Y., Huang, W., Xu, T., and Huang, J. Dropedge: Towards deep graph convolutional networks on node classification. In *International Conference on Learning Representations*, 2020. URL https://openreview.net/forum?id=Hkx1qkrKPr.

Rozemberczki, B., Allen, C., and Sarkar, R. Multi-scale attributed node embedding, 2019. URL https://arxiv.org/abs/1909.13021.

Rusch, T. K., Chamberlain, B. P., Rowbottom, J., Mishra, S., and Bronstein, M. M. Graph-coupled oscillator networks, 2022. URL https://arxiv.org/abs/2202.02296.

Sanchez-Gonzalez, A., Heess, N., Springenberg, J. T., Merel, J., Riedmiller, M., Hadsell, R., and Battaglia, P. Graph networks as learnable physics engines for inference and control. In Dy, J. and Krause, A. (eds.), *Proceedings of the 35th International Conference on Machine Learning*, volume 80 of *Proceedings of Machine Learning Research*, pp. 4470–4479. PMLR, 10–15 Jul 2018. URL https://proceedings.mlr.press/v80/sanchez-gonzalez18a.html.

Scaman, K. and Virmaux, A. Lipschitz regularity of deep neural networks: Analysis and efficient estimation. In *Proceedings of the 32nd International Conference on Neural Information Processing Systems*, NIPS'18, pp. 3839–3848, Red Hook, NY, USA, 2018. Curran Associates Inc.

Shang, C., Tang, Y., Huang, J., Bi, J., He, X., and Zhou, B. End-to-end structure-aware convolutional networks for knowledge base completion. *Proceedings of the AAAI Conference on Artificial Intelligence*, 33 (01):3060–3067, Jul. 2019. doi: 10.1609/aaai.v33i01.33013060. URL https://ojs.aaai.org/index.php/AAAI/article/view/4164.

Shi, C., Xu, M., Zhu, Z., Zhang, W., Zhang, M., and Tang, J. Graphaf: a flow-based autoregressive model for molecular graph generation, 2020.

Sia, J., Jonckheere, E., and Bogdan, P. Ollivier-ricci curvature-based method to community detection in complex networks. *Scientific Reports*, 9(1): 9800, Jul 2019. ISSN 2045-2322. doi: 10.1038/s41598-019-46079-x. URL https://doi.org/10.1038/s41598-019-46079-x.

Topping, J., Giovanni, F. D., Chamberlain, B. P., Dong, X., and Bronstein, M. M. Understanding over-squashing and bottlenecks on graphs via curvature. In *International Conference on Learning Representations*, 2022. URL https://openreview.net/forum?id=7UmjRGzp-A.

van der Hoorn, P., Lippner, G., Trugenberger, C., and Krioukov, D. Ollivier curvature of random geometric graphs converges to ricci curvature of their riemannian manifolds, 2020. URL https://arxiv.org/abs/2009.04306.

Vaswani, A., Shazeer, N., Parmar, N., Uszkoreit, J., Jones, L., Gomez, A. N., Kaiser, L. u., and Polosukhin, I. Attention is all you need. In Guyon, I., Luxburg, U. V., Bengio, S., Wallach, H., Fergus, R., Vishwanathan, S., and Garnett, R. (eds.), *Advances in Neural Information Processing Systems*, volume 30. Curran Associates, Inc., 2017. URL https://proceedings.neurips.cc/paper/2017/file/3f5ee243547dee91fbd053c1c4a845aa-Paper.pdf.

Veličković, P., Cucurull, G., Casanova, A., Romero, A., Liò, P., and Bengio, Y. Graph Attention Networks. *International Conference on Learning Representations*, 2018. URL https://openreview.net/forum?id=rJXMpikCZ.

Wu, Q., Zhang, H., Gao, X., He, P., Weng, P., Gao, H., and Chen, G. Dual graph attention networks for deep latent representation of multifaceted social effects in recommender systems. In *The World Wide Web Conference*, WWW '19, pp. 2091–2102, New York, NY, USA, 2019. Association for Computing Machinery. ISBN 9781450366748. doi: 10.1145/3308558.3313442. URL https://doi.org/10.1145/3308558.3313442.

Xu, K., Li, C., Tian, Y., Sonobe, T., Kawarabayashi, K., and Jegelka, S. Representation learning on graphs with jumping knowledge networks. *CoRR*, abs/1806.03536, 2018. URL http://arxiv.org/abs/1806.03536.

Xu, K., Hu, W., Leskovec, J., and Jegelka, S. How powerful are graph neural networks? In *International Conference on Learning Representations*, 2019. URL https://openreview.net/forum?id=ryGs6iA5Km.

Yang, Y., Wei, Z., Chen, Q., and Wu, L. Using external knowledge for financial event prediction based on graph neural networks. In *Proceedings of the 28th ACM International Conference on Information and Knowledge Management*, CIKM '19, pp. 2161–2164, New York, NY, USA, 2019. Association for Computing Machinery. ISBN 9781450369763. doi: 10.1145/3357384.3358156. URL https://doi.org/10.1145/3357384.3358156.

Yang, Z., Cohen, W. W., and Salakhutdinov, R. Revisiting semi-supervised learning with graph embeddings, 2016. URL https://arxiv.org/abs/1603.08861.

Ying, R., He, R., Chen, K., Eksombatchai, P., Hamilton, W. L., and Leskovec, J. Graph convolutional neural networks for web-scale recommender systems. In *Proceedings of the 24th ACM SIGKDD international conference on knowledge discovery & data mining*, pp. 974–983, 2018.

Zhang, F., Liu, X., Tang, J., Dong, Y., Yao, P., Zhang, J., Gu, X., Wang, Y., Shao, B., Li, R., and Wang, K. Oag: Toward linking large-scale heterogeneous entity graphs. In *Proceedings of the 25th ACM SIGKDD International Conference on Knowledge Discovery amp; Data Mining*, KDD '19, pp. 2585–2595, New York, NY, USA, 2019. Association for Computing Machinery. ISBN 9781450362016. doi: 10.1145/3292500.3330785. URL https://doi.org/10.1145/3292500.3330785.

Zhao, L. and Akoglu, L. Pairnorm: Tackling oversmoothing in gnns. In *International Conference on Learning Representations*, 2020. URL https://openreview.net/forum?id=rkecl1rtwB.

Supplement for "Revisiting Over-smoothing and Over-squashing using Ollivier-Ricci Curvature"

In this supplementary material, we first present how Equation (1) accommodates different designs of GNNs in Appendix A. Then, we discuss the lack of an appropriate measure for the over-squashing issue in Appendix B. Skipped proofs within the main text are provided in Appendix C. We present our experiment settings in Appendix D and describe dataset statistics in Appendix E. Finally, we provide our hardware specifications and list of libraries in Appendix F.

A. Message Passing Neural Networks

In its most general form, a typical layer of a message passing neural network is given by the following update rule (Bronstein et al., 2021):

$$\boldsymbol{H}_u = \phi\left(\boldsymbol{X}_u, \bigoplus_{v\in\mathcal{N}_u} \Lambda(\boldsymbol{X}_u, \boldsymbol{X}_v)\right). \tag{13}$$

Here, Λ , $\bigoplus$ and ϕ are the message, aggregate and update functions. Different designs of MPNNs amount to different choices for these functions. The additional input of $\boldsymbol{X}_u$ to ϕ represents an optional skip-connection.

In practice, we found that the skip connection of each vertex u is often implemented by considering a message passing scheme where each node sends a message to itself. This can be thought of as adding self-loops to the graph, and its impact has been studied by Xu et al. (2018) and Topping et al., (2022). Then, Λ could be realized as a learnable affine transformation ψ of $\boldsymbol{X}_v$, the aggregating function $\bigoplus$ could either be chosen as a sum, mean, weighted mean, or max operation, and ϕ is a suitable activation function. Hence, we arrive at equation 1, which we restate below

$$\boldsymbol{X}_u^{k+1} = \phi_k\left(\bigoplus_{p\in\tilde{\mathcal{N}}_u} \psi_k(\boldsymbol{X}_p^k)\right).$$

For example, graph convolutional network (GCN) (Kipf & Welling, 2017) defines its layer as

$$\boldsymbol{H}_u = \sigma\left(\sum_{v\in\tilde{\mathcal{N}}_u} \frac{1}{c_{uv}}\boldsymbol{W}\boldsymbol{X}_v\right),$$

with $c_{uv} = \sqrt{|\tilde{\mathcal{N}}_u||\tilde{\mathcal{N}}_v|}$. The mean aggregator variant (but not other variants) of GraphSAGE (Hamilton et al., 2017) uses the same formulation but with $c_{uv} = |\tilde{\mathcal{N}}_u|$. Both choices of c_{uv} have the exact same spectral characteristics and act identically in theory (Li et al., 2018a), which leads to an averaging behavior based on node degrees. Similarly, graph attention networks (GAT) (Veličković et al., 2018) defines its single head layer as

$$\boldsymbol{H}_u = \sigma\left(\sum_{v\in\tilde{\mathcal{N}}_u} a_{uv}\boldsymbol{W}\boldsymbol{X}_v\right).$$

The difference here being a_{uv} is now a learnable function given by the attention mechanism (Vaswani et al., 2017). Finally, graph isomorphis network (GIN) (Xu et al., 2019) is formulated by

$$\boldsymbol{H}_u = \mathrm{MLP}\left((1+\epsilon)\boldsymbol{X}_u + \sum_{v\in\mathcal{N}_u} \boldsymbol{X}_v\right),$$

where MLP is a multilayer perceptron. GIN achieves its best performance with the model GIN-0, in which ϵ is set to be 0.

We remark that most nonlinear activation functions such as ReLU, Leaky ReLU, Tanh, Sigmoid, softmax, etc., has a simple and explicit Lipschitz-constant (which equals to 1 more often than not) (Scaman & Virmaux, 2018).

B. Measuring Over-squashing

It is intuitive to think that if N vertices in $\tilde{\mathcal{N}}_u$ contribute to the feature representation of some vertex u by the permutation invariant update rule 1, we should expect each such vertex to provide $\frac{1}{N}$ of the total contribution. If this is repeated over and over, such as in a tree, the exponentially decaying dependence of distant vertices is to be expected. However, quantifying this phenomenon is actually quite difficult.

The first work to call attention to the over-squashing problem (Alon & Yahav, 2021) measures whether breaking the bottleneck improves the results of long-range problems, instead of measuring the decaying importance itself. A definition that took inspiration from the vanishing gradient problem was given by Topping et al. (2022), where it was suggested that $\frac{\partial \boldsymbol{X}_u^k}{\partial \boldsymbol{X}_v^0}$ can be used to evaluate the decreasing importance of distant vertex v to u. However, this definition only works in the one dimensional case, and when $\bigoplus$ is a mean or similar aggregating operators with a natural decaying effect. Such approach does not work if $\bigoplus$ is the sum or max operator simply because the derivative of such aggregator either equals 1 or does not exist entirely. Clearly, it is the *relative* importance of a vertex compared to the contribution of all other vertices that is at the heart of the matter.

To this end, we have found that the closest notion to our description actually predates the observation of the over-squashing issue. Xu et al. (2018) introduced the notion of influence distribution to quantify the relative importance of vertices to each other. It is defined as

$$I_u(v) = \frac{\operatorname{sum}\left(\left[\frac{\partial \boldsymbol{X}_u^k}{\partial \boldsymbol{X}_v^0}\right]\right)}{\sum_{p \in V} \operatorname{sum}\left(\left[\frac{\partial \boldsymbol{X}_u^k}{\partial \boldsymbol{X}_p^0}\right]\right)}$$

where the sum is taken over all entries of each Jacobian matrix. Unfortunately, this definition is quite unwieldy to use in any sort of analysis. We would like to remark that the theoretical proofs in (Xu et al., 2018) are only partially correct. They have made the mistake by claiming

$$\mathbb{E}\left(\frac{X_1}{\sum_{i=1}^n X_i}\right) = \frac{\mathbb{E}(X_1)}{\sum_{i=1}^n \mathbb{E}(X_i)}$$

for i.i.d. random Bernoulli variables X_i.

C. Proofs

In this Appendix, we provide proofs for key results in the paper. We state without proof the following lemma, which can be found in the work of Bourne et al. (2017).

Lemma C.1. *Let μ_1, μ_2 be probability measures on a space V. Then there exists an optimal transport plan π transporting μ_1 to μ_2 with the following property: For all $x \in V$ with $\mu_1(x) \leq \mu_2(x)$, we have $\pi(x, x) = \mu_1(x)$.*

C.1. Proof of Lemma 3.1

Proof. Without loss of generality, assume $n \geq m$. Let π be an optimal transport plan between m_u and m_v satisfying the condition in Lemma C.1. That is, $\pi(p, p) = \frac{1}{n}$ for all $p \in \mathcal{N}(u) \cap \mathcal{N}(v)$. We have

$$\begin{aligned} W_1(m_u, m_v) &= \sum_{p \in \mathcal{N}_u} \sum_{q \in \mathcal{N}_v} \pi(p,q) d(p,q) \\ &= \sum_{\substack{(p,q) \in \mathcal{N}_u \times \mathcal{N}_v \\ p \neq q}} \pi(p,q) d(p,q) + \sum_{p \in \mathcal{N}(u) \cap \mathcal{N}(v)} \pi(p,p) d(p,p). \end{aligned}$$

It is obvious that $d(p, p) = 0$ for any vertex p and $d(p, q) \geq 1$ for any vertices $p \neq q$. We have

$$\begin{aligned} W_1(m_u, m_v) &\geq \sum_{\substack{(p,q) \in \mathcal{N}_u \times \mathcal{N}_v \\ p \neq q}} \pi(p,q) + 0 \\ &= 1 - \sum_{p \in \mathcal{N}_u \cap \mathcal{N}_v} \pi(p,p) \\ &= 1 - \frac{|\mathcal{N}_u \cap \mathcal{N}_v|}{n}. \end{aligned}$$

Hence, we have

$$\frac{|\mathcal{N}_u \cap \mathcal{N}_v|}{\max(m,n)} \geq 1 - W_1(m_u, m_v) = \kappa(u,v).$$

□

C.2. Proof of Theorem 3.2

As ϕ_k is L-Lipschitz, we have

$$\begin{aligned} \left|\boldsymbol{X}_u^{k+1} - \boldsymbol{X}_v^{k+1}\right| &= \left|\phi_k\left(\bigoplus_{p\in\tilde{\mathcal{N}}_u}\psi_k(\boldsymbol{X}_p^k)\right) - \phi_k\left(\bigoplus_{q\in\tilde{\mathcal{N}}_v}\psi_k(\boldsymbol{X}_q^k)\right)\right| \\ &\leq L\left|\bigoplus_{p\in\tilde{\mathcal{N}}_u}\psi_k(\boldsymbol{X}_p^k) - \bigoplus_{q\in\tilde{\mathcal{N}}_v}\psi_k(\boldsymbol{X}_q^k)\right|. \end{aligned} \tag{14}$$

Theorem 3.1 tells us that

$$|\tilde{\mathcal{N}}_v \backslash \tilde{\mathcal{N}}_u| \leq |\tilde{\mathcal{N}}_u \backslash \tilde{\mathcal{N}}_v| = n + 1 - |\mathcal{N}_u \cap \mathcal{N}_v| - 2 \leq n - n\kappa(u,v).$$

Hence, there are at most $\lfloor(1-\kappa(u,v))n\rfloor$ vertices in the extended neighborhood of u that is not present in the extended neighborhood of v and vice versa. The symmetric difference $\tilde{\mathcal{N}}_u \triangle \tilde{\mathcal{N}}_v = (\tilde{\mathcal{N}}_u\backslash\tilde{\mathcal{N}}_v) \cup (\tilde{\mathcal{N}}_v\backslash\tilde{\mathcal{N}}_u)$ satisfies $|\tilde{\mathcal{N}}_u \triangle \tilde{\mathcal{N}}_v| \leq 2(1-\kappa(u,v))n$.

- If $\bigoplus$ is realized as the sum operation, we obtain from equation (14)

$$\begin{aligned} \left|\boldsymbol{X}_u^{k+1} - \boldsymbol{X}_v^{k+1}\right| &\leq L\left|\sum_{p\in\mathcal{N}_u\cup\{u\}}\psi_k(\boldsymbol{X}_p^k) - \sum_{q\in\mathcal{N}_v\cup\{v\}}\psi_k(\boldsymbol{X}_q^k)\right| \\ &= L\left|\sum_{p\in\tilde{\mathcal{N}}_u\backslash\tilde{\mathcal{N}}_v}\psi_k(\boldsymbol{X}_p^k) - \sum_{q\in\tilde{\mathcal{N}}_v\backslash\tilde{\mathcal{N}}_u}\psi_k(\boldsymbol{X}_q^k)\right| \\ &\leq L\sum_{p\in\tilde{\mathcal{N}}_u\triangle\tilde{\mathcal{N}}_v}\left|\psi_k(\boldsymbol{X}_p^k)\right| \\ &\leq (1-\kappa(u,v))2LCMn. \end{aligned}$$

  We can now set $h \equiv 2LCMn$.

- If $\bigoplus$ is realized as the mean operation, we obtain from equation (14)

$$\begin{aligned} \left|\boldsymbol{X}_u^{k+1} - \boldsymbol{X}_v^{k+1}\right| &\leq L\left|\sum_{p\in\tilde{\mathcal{N}}_u}\frac{1}{n+1}\psi_k(\boldsymbol{X}_p^k) - \sum_{q\in\tilde{\mathcal{N}}_v}\frac{1}{m+1}\psi_k(\boldsymbol{X}_q^k)\right| \\ &\leq L\sum_{p\in(\tilde{\mathcal{N}}_u\cap\tilde{\mathcal{N}}_v)}\left(\frac{1}{m+1} - \frac{1}{n+1}\right)\left|\psi_k(\boldsymbol{X}_p^k)\right| \\ &\quad + L\left|\sum_{p\in\tilde{\mathcal{N}}_u\backslash\tilde{\mathcal{N}}_v}\frac{1}{n+1}\psi_k(\boldsymbol{X}_p^k) - \sum_{q\in\tilde{\mathcal{N}}_v\backslash\tilde{\mathcal{N}}_u}\frac{1}{m+1}\psi_k(\boldsymbol{X}_q^k)\right|. \end{aligned} \tag{15}$$

  We have $n \geq m = |\mathcal{N}_v| \geq |\mathcal{N}_u \cap \mathcal{N}_v| \geq \kappa(u,v)n$, and

$$\frac{1}{m+1} - \frac{1}{n+1} \leq \frac{1}{m} - \frac{1}{n} \leq \frac{1}{\kappa(u,v)n} - \frac{1}{n} = \frac{1-\kappa(u,v)}{\kappa(u,v)n}.$$

Therefore, equation (15) gives

$$\begin{aligned}
\left|\boldsymbol{X}_u^{k+1}-\boldsymbol{X}_v^{k+1}\right| &\leq L \sum_{p\in\tilde{\mathcal{N}}_u\cap\tilde{\mathcal{N}}_v} \frac{1-\kappa(u,v)}{\kappa(u,v)n}\left|\psi_k(\boldsymbol{X}_p^k)\right| + L\sum_{p\in\tilde{\mathcal{N}}_u\triangle\tilde{\mathcal{N}}_v}\frac{1}{\kappa(u,v)n+1}\left|\psi_k(\boldsymbol{X}_p^k)\right| \\
&\leq L(n+1)\frac{1-\kappa(u,v)}{\kappa(u,v)n}CM + 2(1-\kappa(u,v))nL\frac{1}{\kappa(u,v)n+1}CM \\
&\leq (1-\kappa(u,v))LCM\left(\frac{n+1}{\kappa(u,v)n}+2\frac{n}{\kappa(u,v)n+1}\right).
\end{aligned}$$

We can now set $h(x)=LCM(\frac{n+1}{xn}+2\frac{n}{nx+1})$.

Clearly, the functions h as defined satisfy the conditions given in Theorem 3.2.

C.3. Proof of Proposition 3.3

We will use proof by induction. For all edges $u\sim v$, repeating the argument in Theorem 3.2, we get $|\tilde{\mathcal{N}}_u \triangle \tilde{\mathcal{N}}_v| \leq 2(1-\delta)n$. Then, the base case $k=1$ follows since

$$\begin{aligned}
|\boldsymbol{X}_u^1-\boldsymbol{X}_v^1| &= \left|\phi_1\left(\frac{1}{n+1}\sum_{p\in\tilde{\mathcal{N}}_u}\psi(\boldsymbol{X}_p)\right)-\phi_1\left(\frac{1}{n+1}\sum_{q\in\tilde{\mathcal{N}}_v}\psi(\boldsymbol{X}_q)\right)\right| \\
&\leq L\left|\frac{1}{n+1}\sum_{p\in\tilde{\mathcal{N}}_u}\psi(\boldsymbol{X}_p)-\frac{1}{n+1}\sum_{q\in\tilde{\mathcal{N}}_v}\psi(\boldsymbol{X}_q)\right| \\
&= \frac{L}{n+1}\left|\sum_{p\in\tilde{\mathcal{N}}_u\setminus\tilde{\mathcal{N}}_v}\psi(\boldsymbol{X}_p)-\sum_{q\in\tilde{\mathcal{N}}_v\setminus\tilde{\mathcal{N}}_u}\psi(\boldsymbol{X}_q)\right| \\
&\leq \frac{L}{n+1}\sum_{p\in\tilde{\mathcal{N}}_u\triangle\tilde{\mathcal{N}}_v}|\psi(\boldsymbol{X}_p)| \\
&\leq \frac{2\lfloor(1-\delta)n\rfloor}{n+1}LCM.
\end{aligned}$$

Suppose the statement is true for k and consider the case $k+1$. We have for all $u\sim v$:

$$\begin{aligned}
\left|\boldsymbol{X}_u^{k+1}-\boldsymbol{X}_v^{k+1}\right| &\leq L\frac{1}{n+1}\left|\sum_{p\in\tilde{\mathcal{N}}_u}\psi_k(\boldsymbol{X}_p^k)-\sum_{q\in\tilde{\mathcal{N}}_v}\psi_k(\boldsymbol{X}_q^k)\right| \\
&= L\frac{1}{n+1}\left|\sum_{p\in\tilde{\mathcal{N}}_u\setminus\tilde{\mathcal{N}}_v}\psi_k(\boldsymbol{X}_p^k)-\sum_{q\in\tilde{\mathcal{N}}_v\setminus\tilde{\mathcal{N}}_u}\psi_k(\boldsymbol{X}_q^k)\right| \\
&\leq LM\frac{1}{n+1}\left|\sum_{p\in\tilde{\mathcal{N}}_u\setminus\tilde{\mathcal{N}}_v}\boldsymbol{X}_p^k-\sum_{q\in\tilde{\mathcal{N}}_v\setminus\tilde{\mathcal{N}}_u}\boldsymbol{X}_q^k\right|. \qquad (16)
\end{aligned}$$

For each $p\in\tilde{\mathcal{N}}_u\backslash\tilde{\mathcal{N}}_v$, match it with one and only one $q\in\tilde{\mathcal{N}}_u\backslash\tilde{\mathcal{N}}_v$. For any node pair (p,q), they are connected by the path $p\sim u\sim v\sim q$, where the difference in norm of features at layer k of each 1-hop connection is at most $\frac{2}{3}C\left(\frac{3M\lfloor(1-\delta)n\rfloor}{n+1}\right)^k$. Hence, we have

$$|\boldsymbol{X}_p^k-\boldsymbol{X}_q^k| \leq 2C\left(\frac{3LM\lfloor(1-\delta)n\rfloor}{n+1}\right)^k.$$

Substituting this into equation (16), and by noting that there are at most $\lfloor(1-\delta)n\rfloor$ pairs, we get

$$\begin{aligned}|\boldsymbol{X}_u^{k+1}-\boldsymbol{X}_v^{k+1}| &\leq LM\frac{1}{n+1}\sum_{(p,q)}|\boldsymbol{X}_p^k-\boldsymbol{X}_q^k|\\ &\leq LM\frac{1}{n+1}\lfloor(1-\delta)n\rfloor 2C\left(\frac{3LM\lfloor(1-\delta)n\rfloor}{n+1}\right)^k\\ &=\frac{2}{3}C\left(\frac{3LM\lfloor(1-\delta)n\rfloor}{n+1}\right)^{k+1}.\end{aligned}$$

By induction, we have shown inequality (8) holds for all $k\geq 1$ and $u\sim v$.

It is known that if the curvatures of all edges in a graph are positive and bounded away from zero by $\delta>0$ then the diameter of the graph does not exceed $\lfloor 2/\delta\rfloor$ (Paeng, 2012). Hence, for any two nodes $u,v\in\mathcal{V}$, the shortest path between them is of length at most $\lfloor 2/\delta\rfloor$. Apply the inequality (8) for each pair of neighboring nodes on this shortest path, we obtain the inequality (9).

C.4. Proof of Proposition 3.4

Note that S consists of elements of the form (p,q) where either $p=q$ or $p\neq q$. The first type corresponds to mutual neighbors of u,v, while the second type corresponds to neighbors of u,v that share an edge. Denote the number of edges of the first type as n_0 and the number of edges of the second type as n_1. A transport plan π between m_u and m_v can be obtained as followed.

- For every vertex p such that $(p,p)\in S$, the mass of $m_u(p)=\frac{1}{n}$ remains in place at p with cost $\pi(p,p)\times 0=\frac{1}{n}\times 0=0$
- For each edge $(p,q)\in S$ with $p\neq q$, transport the mass of $\frac{1}{n}$ from p to q with cost $\pi(p,q)\times 1=\frac{1}{n}\times 1=\frac{1}{n}$. The assumption that each vertex w is a vertex of at most $\frac{n}{m}$ edges ensures that the total mass transported to each vertex is no greater than $\frac{1}{m}$.
- The remaining mass is $1-n_0\frac{1}{n}-n_1\frac{1}{n}$. Transport this amount arbitrarily to obtain a valid optimal transport plan.

This transport plan has cost

$$\sum_{p\in\tilde{\mathcal{N}}_u}\sum_{q\in\tilde{\mathcal{N}}_v}\pi(p,q)d(p,q)\leq n_0 0+n_1\frac{1}{n}+\left(1-n_0\frac{1}{n}-n_1\frac{1}{n}\right)3=3-3n_0\frac{1}{n}-2n_1\frac{1}{n}.$$

We have

$$\kappa(u,v)=1-W_1(m_u,m_v)\geq 1-\left(3-3n_0\frac{1}{n}-2n_1\frac{1}{n}\right)=-2+\frac{3n_0+2n_1}{n}.$$

Therefore, we obtain

$$|S|=n_0+n_1\leq\frac{n}{2}\frac{3n_0+2n_1}{n}\leq n\frac{\kappa(u,v)+2}{2}.$$

We can observe from the proof that a stronger result holds: $3n_0+2n_1\leq n(\kappa(u,v)+2)$.

C.5. Proof of Theorem 3.5

Since ϕ_k and ψ_k are linear operators for all k, their Jacobians J_{ϕ_k},J_{ψ_k} are constant matrices. By inspection of Equation 1, we see that a vertex $w\in V$ can only transmit a message to u if there exists a vertex w' such that $w'\in\tilde{\mathcal{N}}_u\cap\tilde{\mathcal{N}}_w$. Moreover, the chain rule gives

$$\left[\frac{\partial\boldsymbol{X}_u^{k+2}}{\partial\boldsymbol{X}_w^k}\right]=\sum_{w'\in\tilde{\mathcal{N}}_u\cap\tilde{\mathcal{N}}_w}\left[\frac{\partial\boldsymbol{X}_u^{k+2}}{\partial\boldsymbol{X}_{w'}^{k+1}}\right]\left[\frac{\partial\boldsymbol{X}_{w'}^{k+1}}{\partial\boldsymbol{X}_w^k}\right]=\sum_{w'\in\tilde{\mathcal{N}}_u\cap\tilde{\mathcal{N}}_w}J_{\phi_{k+1}}J_{\psi_{k+1}}J_{\phi_k}J_{\psi_k}.$$

Therefore, $\left[\frac{\partial\boldsymbol{X}_u^{k+2}}{\partial\boldsymbol{X}_w^k}\right]$ is the number of distinct paths (that might contain self-loops) from w to u times $J_{\phi_{k+1}}J_{\psi_{k+1}}J_{\phi_k}J_{\psi_k}$.

Table 4. SDRF's best hyper-parameters settings.

	GCN			GIN		
DATASET	# ITERATION	C^+	# REWIRED	# ITERATION	C^+	# REWIRED
CORA	12	0	24	50	∞	50
CITESEER	175	∞	175	25	∞	25
TEXAS	87	0	174	37	0	74
CORNELL	100	0	200	25	0	50
WISCONSIN	25	0	50	150	∞	150
CHAMELEON	50	0	100	87	0	174
ENZYMES	15	0	30	5	0	10
IMDB	10	0	20	10	∞	10
MUTAG	20	∞	20	10	0	20
PROTEINS	5	0	10	15	0	30

Table 5. FoSR's best iteration count settings.

DATASET	GCN	GIN
CORA	150	50
CITESEER	100	200
TEXAS	50	150
CORNELL	125	75
WISCONSIN	175	25
CHAMELEON	50	25
ENZYMES	40	5
IMDB	5	20
MUTAG	10	20
PROTEINS	30	10

The number of distinct paths without self-loops from $q \in \tilde{\mathcal{N}}_v \backslash \{u\}$ to u is not greater than $|S|$ as defined in Proposition 3.4. With self-loops, this rises to at most $|S| + 2$, which corresponds to the case where $q \sim u$.

On the other hand, $\sum_{w \in V} \left[\frac{\partial \boldsymbol{X}_u^{k+2}}{\partial \boldsymbol{X}_w^k} \right]$ equals the number of distinct paths with self-loops with one end at u times $J_{\phi_{k+1}} J_{\psi_{k+1}} J_{\phi_k} J_{\psi_k}$. Clearly, we have

$$\sum_{w \in V} \left[\frac{\partial \boldsymbol{X}_u^{k+2}}{\partial \boldsymbol{X}_w^k} \right] = \left(\sum_{w \in \tilde{\mathcal{N}}_u} (\deg(w) + 1) \right) J_{\phi_{k+1}} J_{\psi_{k+1}} J_{\phi_k} J_{\psi_k}.$$

Let

$$\alpha = \frac{|S| + 2}{\sum_{w \in \tilde{\mathcal{N}}_u} (\deg(w) + 1)},$$

then Proposition 3.4 gives us the required inequality. We can choose β by the same process.

D. Experiment Settings

D.1. Rewiring hyper-parameters

We report the best rewiring settings for every task and baseline GNN architecture. For SDRF, we set the temperature $\tau = \infty$ and only tuned the Ric upper bound C^+ and iteration count. For FoSR, we tuned the iteration count. For BORF, we tuned the number of batches n, number of edges added per batch h, and number of edges removed per batch k. The exact hyper-parameters for SDRF, FoSR and BORF are available in Table 4, Table 5, and Table 6, respectively. We also report the total amount of edges each method rewired, which equals the total number of added and removed connections for SDRF and BORF. The number of edges rewired by FoSR is the same as the iteration count.

Table 6. BORF's best hyper-parameters settings.

	GCN				GIN			
DATASET	n	h	k	# REWIRED	n	h	k	# REWIRED
CORA	3	20	10	90	3	20	30	150
CITESEER	3	20	10	90	3	10	20	90
TEXAS	3	30	10	120	1	20	10	30
CORNELL	2	20	30	100	3	10	20	90
WISCONSIN	2	30	20	100	2	50	30	160
CHAMELEON	3	20	20	120	3	30	30	180
ENZYMES	1	3	2	5	3	3	1	12
IMDB	1	3	0	3	1	4	2	6
MUTAG	1	20	3	23	1	3	1	4
PROTEINS	3	4	1	15	2	4	3	14

Table 7. Architecture settings for node and graph classification tasks.

TASK	DROP-OUT PROBABILITY	#GNN LAYERS	HIDDEN DIMENSIONS	FINAL ACTIVATION
NODE	0.5	3	128	RELU
GRAPH	0.5	4	64	RELU

D.2. Architecture and experiment settings

For graph and node classification, we utilized fixed model architectures with fixed numbers of GNN layers across all datasets. We used 3 GNN layers for node classification and 4 for graph classification tasks. All the intermediate GNN layers (except for the input and output layer) have the same number of input and output dimensions specified by the hidden dimensions. At the end of all the GNN layers, we also added a drop-out layer with a fix drop-out probability and a final activation layer. The specific hidden dimensions, drop-out probabilities and final activation layers for both node and graph classification tasks are specified in the architecture settings in Table 8.

For each graph and node classification experiment, we randomly split the dataset into train, validation and test sets 100 times corresponding to 100 trials. For each trial, the GNN model is trained on the train set using the Adam optimizer and validated using the validation set. The test accuracy corresponding to the best accuracy on the validation set is recorded as the test accuracy of the current trial. After all 100 trials are finished, the mean test accuracy and the 95% confidence interval across all trials are computed and recorded in Tables 2 and 3. We also implemented a callback that stops the training process upon no improvement on the validation accuracy for 100 epochs. The train and validation fractions used to split the dataset is specified in Table 7.

Table 8. Experiment settings for node and graph classification tasks (Note: The train fraction is with respect to the entire dataset while the validation fraction is with respect to the train set).

TASK	LEARNING RATE	#TRIALS/RUN	STOP PATIENCE	TRAIN FRACTION	VALIDATION FRACTION
NODE	0.001	100	100	0.6	0.2
GRAPH	0.001	100	100	0.8	0.1

E. Dataset Statistics

We provide a summary of statistics of all datasets used in Table 9 and Table 10. We also report the mean and standard deviation of the Ollivier Ricci curvature for each dataset. On node classification tasks, this is exactly the statistics of the set of edge curvature values. On graph classification tasks, this is the statistics of the mean curvature value of all graphs within the dataset.

Table 9. Statistics of node classification datasets.

	CORNELL	TEXAS	WISCONSIN	CORA	CITESEER	CHAMELEON
#NODES	140	135	184	2485	2120	832
#EDGES	219	251	362	5069	3679	12355
#FEATURES	1703	1703	1703	1433	3703	2323
#CLASSES	5	5	5	7	6	5
DIRECTED	TRUE	TRUE	TRUE	FALSE	FALSE	TRUE
ORC MEAN	-0.39	-0.24	-0.59	-0.19	-0.31	0.64
ORC STD	0.52	0.45	0.71	0.68	0.78	0.58

Table 10. Statistics of graph classification datasets.

	ENZYMES	IMDB	MUTAG	PROTEINS
#GRAPHS	600	1000	188	1113
#NODES	2-126	12-136	10 - 28	4-620
#EDGES	2 - 298	52 - 2498	20 - 66	10 - 2098
AVG #NODES	32.63	19.77	17.93	39.06
AVG #EDGES	124.27	193.062	39.58	145.63
#CLASSES	6	2	2	2
DIRECTED	FALSE	FALSE	FALSE	FALSE
ORC MEAN	0.13	0.58	-0.27	0.17
ORC STD	0.15	0.19	0.05	0.20

Table 11. Server specifications for conducting all experiments.

SERVER ID	COMPONENTS	SPECIFICATIONS
	ARCHITECTURE	X86 64
	OS	UBUNTU 20.04.5 LTS X86$_6$4
1	CPU	INTEL I7-10700KF (16) @ 5.100GHZ
	GPU	NVIDIA GEFORCE RTX 2080 TI REV. A
	RAM	12GB
	ARCHITECTURE	X86 64
	OS	UBUNTU 20.04.5 LTS X86$_6$4
2	CPU	AMD EPYC 7742 64-CORE
	GPU	NVIDIA A100 TENSOR CORE
	RAM	40GB

F. Hardware Specifications and Libraries

All experiments were implemented in Python using PyTorch, Numpy, PyG (PyTorch Geometric), POT (Python Optimal Transport) with figures created using TikZ. PyTorch, PyG and NumPy are made available under the BSD license, POT under MIT license, and TikZ under the GNU General Public license.

We conducted our experiments on two local servers with the specifications laid out in Table 11.